Influence of the Phase State of Self-Assembling Redox Mediators on their Electrochemical Activity

John P. E. Muller and Burcu S. Aytar
Dept. of Chemical and Biological Engineering, University of Wisconsin-Madison, Madison, WI 53706

Yukishige Kondo
Dept. of Industrial Chemistry, Tokyo University of Science, Tokyo, Japan

David M. Lynn and Nicholas L. Abbott
Dept. of Chemical and Biological Engineering, University of Wisconsin-Madison, Madison, WI 53706

DOI 10.1002/aic.14402
Published online March 4, 2014 in Wiley Online Library (wileyonlinelibrary.com)

Self-assembling redox mediators have the potential to be broadly useful in a range of interfacial electrochemical contexts because the oxidation state and state of assembly of the mediator are closely coupled. In this article, we report an investigation of the self-assembly of single- and double-tailed ferrocenyl amphiphiles [(11-ferrocenylundecyl)trimethylammonium bromide (FTMA) and bis(11-ferrocenylundecyl)dimethylammonium bromide (BFDMA), respectively] at the surfaces of Pt electrodes and the impact of the dynamic assembled state of the amphiphiles on their rate of oxidation. We conclude that frozen aggregates of BFDMA adsorb to the surfaces of the Pt electrodes, and that slow dynamics of reorganization of BFDMA within these aggregates limits the rate of electrooxidation of BFDMA. In contrast, FTMA, while forming assemblies on the surfaces of Pt electrodes, is characterized by fast reorganization dynamics and a corresponding rate of oxidation that is an order of magnitude greater than BFDMA. © 2014 American Institute of Chemical Engineers *AIChE J*, 60: 1381–1392, 2014
Keywords: redox, surfactant, self-assembly, interfaces, electrochemical

Introduction

Redox-active amphiphiles, when adsorbed at surfaces, can be used to modify interfacial electron transfer events in a wide range of contexts. For example, adsorbed surfactants can enable fast electron transfer through molecular bridges over large distances for use in biosensors,[1,2] organic light-emitting diodes,[3–5] and molecular electronic devices.[6,7] Alternatively, surfactants can block the surface of an electrode to inhibit corrosion[8,9] or the poisoning of an electrocatalyst.[10] Finally, surfactants can change the surface of an electrode from being hydrophilic to hydrophobic and thereby modify the potential for oxidation of water and provide a wider potential window for transformations of organic compounds.[11] In the majority of systems, a key underlying fundamental issue is how the dynamical organization of the amphiphiles impacts interfacial electron transfer processes.

In an effort to understand how the dynamics and organization of amphiphiles impact electron transfer processes at interfaces, several prior studies have reported investigations of rates of electron transfer from electroactive groups [e.g., ferrocene (Fc)] held at a fixed distance from the surface of an electrode by using highly organized, self-assembled monolayers.[12–16] Consistent with the so-called superexchange model[17] (fast single electron tunneling steps through molecular bridges), the rate constants for electron transfer were measured in these studies to decrease exponentially with increasing distance over which electron transfer took place.[18,19] Alternatively, and of relevance to the study reported in this article, Rusling and coworkers have studied the distance dependence of electron-transfer rate constants using ferrocene and ferrocenyl amphiphiles coadsorbed with cetyltrimethylammonium bromide on the surfaces of electrodes. They interpreted their results to indicate that an increase in distance of approximately 2 Å between the ferrocene and electrode resulted in an order of magnitude decrease in the rate of electron transfer.[20] Building from these prior studies, we report here an investigation of how the self-assembled states of amphiphilic redox mediators impact their interfacial electrochemical behaviors. Specifically, we compare and contrast the properties of two water-soluble amphiphiles, (11-ferrocenylundecyl)trimethylammonium bromide (FTMA) and bis(11-ferrocenylundecyl)dimethylammonium bromide (BFDMA; Figure 1), that form significantly different self-assembled structures in solution and, as demonstrated in our study, at electrode surfaces.

The ferrocenyl amphiphiles used in our study have been investigated over the past decade as the basis of redox-active

Additional Supporting Information may be found in the online version of this article.

Correspondence concerning this article should be addressed to D. M. Lynn at dlynn@engr.wisc.edu or N. L. Abbott at abbott@engr.wisc.edu.

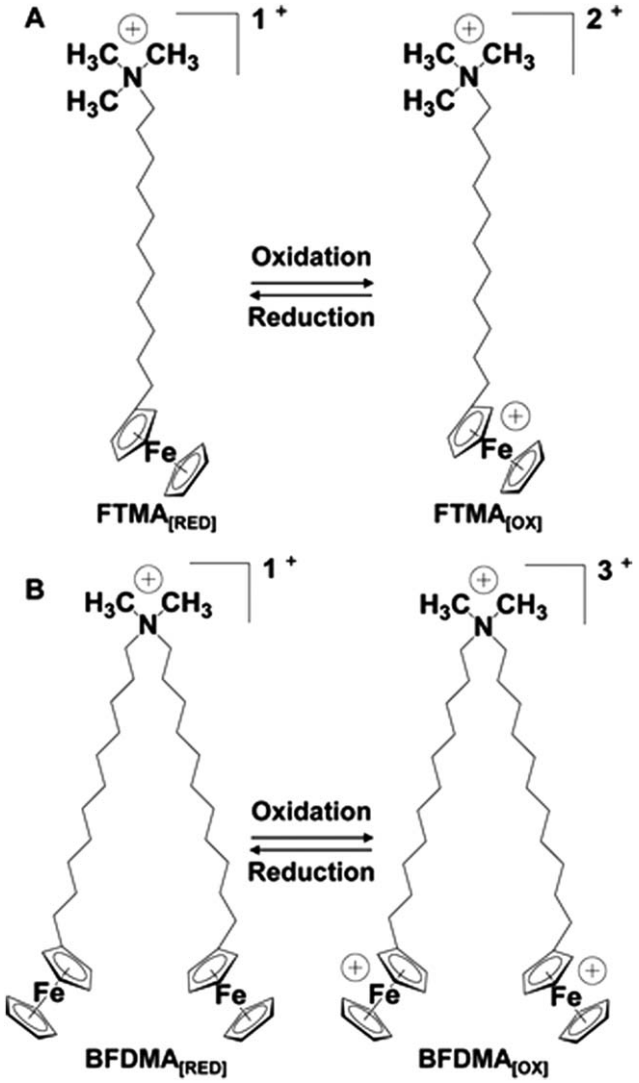

Figure 1. Structures of (A) FTMA (11-ferrocenylundecyl)trimethylammonium bromide) and (B) BFDMA (bis(11-ferrocenylundecyl)dimethylammonium bromide).

surfactant systems that can be placed under active control (i.e., enabling tuning of the amphiphilic nature of surfactants through cycling of the molecules between "on" and "off" redox states).[21] In particular, the single-tailed redox-active ferrocenyl amphiphile FTMA (Figure 1A) was used to demonstrate that changes in the oxidation state of ferrocene within the amphiphile can lead to large changes in surface tensions of aqueous solutions,[22,23] the reversible assembly and disassembly of micelles in solution,[24] and active control over the interactions of surfactants with macromolecules.[25] In addition, the double-tailed redox-active amphipihilic surfactant BFDMA (Figure 1B) has been shown to form complexes (or lipoplexes) with DNA that can deliver DNA to cells with an efficiency that depends strongly on the oxidation state of the ferrocenyl groups.[26–33] Although both of these amphiphiles have been investigated extensively in bulk solution (including characterization of their critical micelle concentrations (CMCs); see below[21]), how their dynamic self-assembly at surfaces impacts their electrochemical activity has not been investigated in detail, particularly for BFDMA. Knowledge of the factors that control the rates of oxidation of these species at electrodes will be broadly useful for the rational design of systems containing self-assembling redox-active molecules. In this article, as a first step toward this goal, we compare and contrast the electrochemical characteristics of BFDMA and FTMA at a Pt electrode.

A central goal of the study reported in this article was to understand how the differences in the self-assembled states of amphiphilic redox-active species impact the rates of oxidation and reduction of the amphiphiles at electrodes. Here, we note that we have previously observed that the rate of oxidation of BFDMA is slow relative to FTMA.[24,34–37] For FTMA, it has been proposed in past studies that, within a concentration boundary layer formed at an electrode held at oxidizing overpotentials, small globular micelles of FTMA present in bulk solution disassemble prior to arriving at the electrode.[35–37] In contrast to FTMA, BFDMA forms large aggregates in solution even at low concentrations.[31] In addition, the dynamics of disassembly of BFDMA are expected to be much slower than FTMA. We hypothesized that the sizes and/or dynamics of the assemblies formed by BFDMA relative to FTMA in solution underlie their striking differences in electrochemical activity. To test this hypothesis, we used cyclic voltammetry (CV) at stationary electrodes and linear sweep voltammetry at rotating disk electrodes (RDEs) to provide insight into the physical processes occurring at electrodes incubated in aqueous solutions of BFDMA and FTMA. Our results reveal that the dynamics of the self-assembled states of the ferrocenyl amphiphiles have a pronounced impact of the rates of electron transfer to and from electrodes. Overall, the results presented in this article hint that redox-active amphiphiles may offer the basis of self-assembling redox mediators that can be used to tune electron transfer events via changes in self-assembly (including redox-induced changes in self-assembly). Such principles have the potential to be broadly useful in designing interfacial charge transfer processes involved, for example, in energy storage and light-harvesting processes (e.g., photocatalytic splitting of water or solar cells).

Materials and Methods

Materials

FTMA was purchased from Dojindo Corporation (Gaithersburg, MD) and was used without further purification. BFDMA was synthesized according to methods published elsewhere.[31,32] Lithium sulfate monohydrate was purchased from Sigma-Aldrich (St. Louis, MO). Deionized water (18.2 MΩ) was used to prepare all salt solutions.

Methods

Sample Preparation. Each surfactant was dissolved in 20 mL aqueous 1 mM Li_2SO_4 (pH 5.1). FTMA solutions (1 mM) dissolved readily but 1 mM BFDMA solutions required sonication for 20 min. Solutions were deoxygenated by bubbling argon for 30 min before use. An amphiphile concentration of 1 mM and electrolyte composition of 1 mM Li_2SO_4 was used for both BFDMA and FTMA throughout the experiments. These conditions were selected for relevancy to prior studies, where bulk oxidation of BFDMA was previously performed.[27–30,33,38–40]

Bulk Electrolysis. Bulk electrolysis was performed using an AFCBP1 Bipotentiostat (Pine Instrument Company,

Grove City, PA). The working and counter electrodes were 25 × 25 mm^2 platinum 45 mesh, woven from 0.198-mm diameter wire, 99.9% (metals basis), folded twice into a 12.5 × 12.5 mm^2, four-layered square (Alfa Aesar, Ward Hill, MA). Prior to use, the electrodes were polarized cathodically in 1.0 N H_2SO_4 to evolve H_2 by applying 200 potential sweeps of 0 to −1 V [vs. a silver|silver chloride (Ag|AgCl) reference electrode (BASi, West Lafayette, IN)] to remove oxides from the surface of the electrodes.[41] Bulk oxidation of FTMA and BFDMA was performed at either 0.4 or 0.6 V, respectively, (vs. Ag|AgCl), at 25°C with continuous stirring. The process of oxidation was stopped when a constant current was passed at the working electrode for at least 30 min. UV-vis spectrophotometry[42] and integration of the current vs. time plots were used to determine the extent of oxidation of each amphiphile. We note that the electrochemical experiments reported in this article were performed at pH 5.1, and that the counter electrode reaction likely involves the reduction of H^+/water.

CV at Stationary Electrodes and Linear Sweep Voltammetry at RDEs. A 5-mm diameter disk working electrode (Pt) was used for all stationary and RDE experiments. The electrode was polished using alumina polishing gamal, grade B (Fisher Chemical, Pittsburgh, PA) and degreased with acetone. Prior to use, the electrode was then polarized cathodically (as described above). These cleaning steps were performed as described in previous studies[41] and they were found to provide reproducible results. Measurements performed using a RDE used an ASR speed control and an analytical rotator (Pine Instrument Company, Grove City, PA) to provide specific rotational speeds of the working electrode. Finally, prior to recording CVs, each electrode was swept from 0 mV to either 400 mV for FTMA or 600 mV for BFDMA (vs. Ag|AgCl) at a scan rate of 100 mV/s until there was no further change in the magnitudes of anodic or cathodic Faradaic peak currents on subsequent scans. This electrode conditioning step was found to be necessary to obtain consistent and reproducible results.

The peak cathodic and anodic currents (i_{peak}) measured in CVs obtained using the stationary disk electrode were analyzed to determine the rate-limiting electrode processes. For mass transfer-limited, reversible processes at the electrode (no adsorption), the current passed at the electrode was analyzed using the Randles–Sevcik equation[43]

$$i_{peak,\,a\,or\,c} = 0.4463 n^{3/2} \left(\frac{F^3}{RT}\right)^{1/2} A D_O^{1/2} \upsilon^{1/2} C_o^* \qquad (1)$$

where n is the number of electrons in the half cell reaction, R is the ideal gas constant, T is the temperature of the solution, F is Faraday's constant, A is the area of working electrode, D_o is the diffusion coefficient of the dissolved electroactive species, C_O^* is the bulk concentration of the electroactive species, and υ is the scan rate of the applied potential. According to Eq. 1, when mass transport is rate-limiting, i_{peak} is proportional to $\upsilon^{1/2}$. This relationship is true when sweeping the potential either anodically (producing a peak current, $i_{peak,a}$) or cathodically (producing a peak current, $i_{peak,c}$). Alternatively, if only adsorbed species lead to the current passed at the working electrode, the peak anodic or cathodic current, i_{peak}, becomes[44]

$$i_{peak,\,a\,or\,c} = \left(\frac{n^2F^2}{4RT}\right) A \upsilon \Gamma_o^* \qquad (2)$$

where Γ_o^* is the concentration of adsorbed electrochemically active species at the electrode surface. For this physical situation, i_{peak} is proportional to υ. The linear sweep voltammetry was performed at a RDE of known area, A, and analyzed using the Levich equation[45,46]

$$i_{l,c} = 0.620 n F A D_O^{2/3} \omega^{1/2} \upsilon^{-1/6} C_O^* \qquad (3)$$

where υ is now the kinematic viscosity of the solution and the speed of the RDE is ω.[46] Analysis of measurements obtained at both stationary and RDEs were analyzed to provide estimates of the diffusion coefficient, D_o. The Stokes–Einstein equation was used to calculate the apparent hydrodynamic radius of the aggregates according to

$$D_o = \frac{k_B T}{6\pi\eta R_H} \qquad (4)$$

where R_H is the apparent hydrodynamic radius, η is the viscosity, T is temperature, and k_B is Boltzmann's constant.

Dynamic Light Scattering. Dynamic light scattering (DLS) measurements of bulk solutions of 1 mM FTMA and 1 mM BFDMA were performed using a 100 mW, 532-nm laser (Coherent Compass 315M-100) and a BI-9000AT digital autocorrelator (Brookhaven Instruments Corporation, Holtsville, NY) at temperatures from 25 to 75°C. The scattering of light was measured at 90°. The autocorrelation functions were analyzed using CONTIN.[47,48]

Differential Scanning Calorimetry. Differential scanning calorimetry (DSC) measurements of bulk solutions of 1 mM FTMA and 1 mM BFDMA were performed using a Q100 modulated differential scanning calorimeter with autosampler and mass flow control (TA Instruments, New Castle, DE). Samples (7 ± 1 mg), hermetically sealed in aluminum pans, were allowed to equilibrate at 25°C before ramping the temperature at a rate of 1°C/min up to 85°C. The samples were held for 2 min at this temperature and then cooled at 1°C/min to 25°C.

Results and Discussion

Bulk electrolysis of BFDMA and FTMA

We begin by reporting an experiment that aimed to quantify differences in the rates of electrochemical oxidation of BFDMA and FTMA under the same experimental conditions (25°C, 1 mM of amphiphile in 4.5 mL). As discussed in the Introduction, the pronounced differences that we measured in the rates of oxidation of these two ferrocenyl amphiphiles motivated the investigation that is reported in the remainder of this article. This initial experiment involved application of an oxidizing potential of either 0.4 or 0.6 V (vs. Ag|AgCl) to Pt mesh electrodes immersed in solutions of FTMA or BFDMA, respectively. These oxidizing potentials were chosen on the basis of prior studies of FTMA[34,36] and BFDMA[27,28,31–33] which showed that application of these potentials leads to complete oxidation of each amphiphile. As detailed later in this article, under these conditions, the overpotential (applied potential minus formal potential, E^o) applied to the Pt electrodes is similar (within 0.04 V) for the two amphiphiles, and, therefore, the driving force for oxidation of each amphiphile is similar (E^o was determined for FTMA to be 0.140 ± 0.010 V (vs. Ag|AgCl) and for

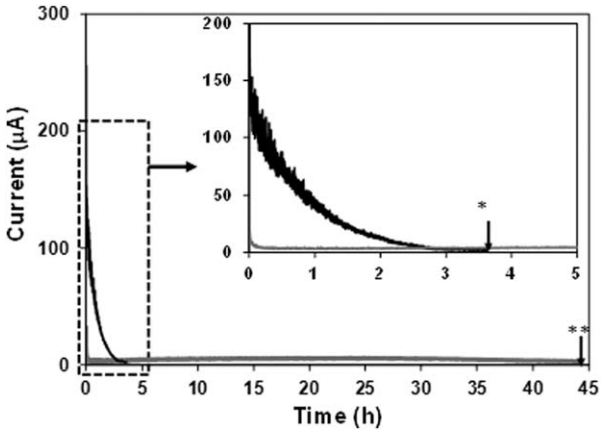

Figure 2. Current passed during electrochemical oxidation of 1 mM $FTMA_{RED}$ (black line, at 0.4 V) or 1 mM $BFDMA_{RED}$ (gray line, at 0.6 V) in 1 mM Li_2SO_4 pH 5 at ambient temperature.

Platinum mesh working and counter electrodes and a Ag|AgCl reference electrode were used. The volume of the solution was 4.5 mL.

BFDMA to be 0.305 ± 0.004 V (vs. Ag|AgCl) from the CV experiments described later).

Figure 2 shows the current passed at a Pt mesh electrode, measured as a function of time, for both FTMA and BFDMA. Inspection of Figure 2 reveals striking differences in the electrochemical behaviors of the two amphiphiles. First, the initial current passed during oxidation of FTMA was approximately 250 μA, compared to only 32 μA for BFDMA (see inset in Figure 2). Correspondingly, whereas the current passed at the electrode immersed into the solution of FTMA decayed over 3.6 h (Figure 2, black line), a sustained but smaller current was observed over almost 45 h when using BFDMA (Figure 2, gray line). Finally, we note that the current passed during oxidation of FTMA dropped gradually at a rate of approximately 50 μA per hour over the duration of the experiment, whereas for BFDMA, the current dropped below 10 μA within the first few minutes of application of the electrical potential. These initial observations provided the first hint that a barrier involving an adsorbed layer of BFDMA may be forming at the electrode immersed into the BFDMA solution.

To explore further the hypothesis that BFDMA was forming a barrier at the electrode, in an independent experiment that was otherwise identical to the experiment shown in Figure 2, a solution of BFDMA was incubated against the Pt mesh working electrode for 1 h before applying an oxidizing potential of 0.6 V (vs. Ag|AgCl, see Supporting Information Figure S1). Although the initial current passed at this electrode was 32 μA (unchanged from that measured above), the total charge passed over the first 400 s of the experiment was 30% less than that measured without preincubation of the electrode in the BFDMA solution (2.5 and 3.6 mC, respectively). This result provides further support for our hypothesis that BFDMA forms an assembly on the electrode surface that slows oxidation of the amphiphile.

We integrated the currents shown in Figure 2 over time to determine the total charge passed during the bulk electrolyses of FTMA and BFDMA and use the total charge to calculate the extent of oxidation of the ferrocenyl amphiphiles in solution. From these calculations, we determined that the charge passed at the electrode immersed into the FTMA solution was 0.396 C (corresponding to 91% of the theoretical charge for complete oxidation of all FTMA molecules in solution) and the charge passed at the electrode immersed into the BFDMA solution was 0.812 C (corresponding to 94% of the theoretical charge for complete oxidation of all BFDMA molecules in solution). We note also that the charge passed using BFDMA is approximately twice the value for FTMA, consistent with oxidation of both ferrocene groups of BFDMA. Overall, from these electrochemical measurements, we conclude that, although the oxidation of BFDMA is slower than FTMA, the oxidation of both amphiphiles was largely complete at the end of the experiments reported in Figure 2. This conclusion was supported additionally by measurements using UV-vis absorption spectrophotometry performed on each amphiphile solution before and after oxidation (see Supporting Information Figure S2).

CV at *stationary electrodes*

To provide further insight into the physical processes that underlie the observations in Figure 2, we performed CV at a stationary Pt electrode immersed into solutions of either FTMA (Figures 3A, B) or BFDMA (Figures 3C, D). Similar to Figure 2, these measurements were performed in 1 mM Li_2SO_4 solution at room temperature. The range of potentials over which CVs were performed was 0–400 mV (vs. Ag|AgCl) for FTMA and 0–600 mV (vs. Ag|AgCl) for BFDMA [i.e., from 0 mV to the potential used for the bulk electrolysis of the amphiphiles (see Figure 2)]. The voltage scan rates were increased from 10 to 200 mV/s to determine the dependence of the peak current on scan rate for each amphiphile (Figures 3B, D). Below, we make three observations regarding the data reported in Figure 3.

First, for FTMA, we measured two cathodic and two anodic Faradaic current peaks at all scan rates (Figure 3A). The magnitude of the peak at the lowest potential (for scans in both directions) was found to depend on the scan rate with an exponent of 0.50 ± 0.01 (Figure 3B, peaks labeled a and c, correlation coefficient, $R^2 > 0.99$, $n = 2$). This result suggests that these peaks in the CV are caused by FTMA that is diffusing from solution to the electrode where it is oxidized (Eq. 1). In contrast, the second peaks (at higher potential) in the CVs recorded for FTMA depend on the scan rate with an exponent of 1.00 ± 0.01 (Figure 3B, peaks labeled b and d, correlation coefficient, $R^2 > 0.99$, $n = 2$). These peaks in the CV, therefore, appear to be due to FTMA that is adsorbed at the electrode surface (Eq. 2). Overall, the occurrence of the second Faradaic current peak in both anodic and cathodic scan directions (following the initial peak current corresponding to diffusing species, i.e., postpeaks) indicates that FTMA adsorption at the electrode surface causes a substantial increase in the free energy required to change the oxidation state of the FTMA (relative to freely diffusing FTMA).[49] Specifically, with reference to the CV measured at a scan rate of 200 mV/s (black data, Figure 3A), the peak currents for the adsorbed species occur at 0.325 V (vs. Ag|AgCl) in the anodic direction and 0.195 V (vs. Ag|AgCl) in the cathodic direction. In contrast, the potentials at which the current peaks for the diffusing species are 0.226 V (vs. Ag|AgCl) in the anodic direction and 0.081 V (vs. Ag|AgCl) in the cathodic direction. By using the Nernst equation,[50] the effect of adsorption on the free energy required to change the oxidation state of FTMA was

estimated to be 3.9 ± 0.8 kT for the anodic scan direction, and 4.4 ± 0.8 kT for the cathodic scan direction at 200 mV/s. Similar conclusions are reached using the data presented in Figure 3A at other scan rates.

In contrast to FTMA, we measured only a single peak in the CVs for solutions of BFDMA [in both scan directions (Figure 3C)]. The dependence of the magnitude of the peak current on scan rate was characterized by an exponent of 0.57 ± 0.12 during oxidation and 0.67 ± 0.10 during reduction ($n = 3$, Figure 3D), suggesting that the peak current contained contributions from both diffusing and adsorbed species. We interpret these CVs with a single peak in either scan direction to indicate that the free energy required to change the oxidation states of the "bound" and "diffusing BFDMA species" are not measurably different. Here, we note that Kakizawa et al.[32] observed the presence of only one peak when oxidizing BFDMA at a Pt electrode (using 5 mM BFDMA at 20 mV/s), which they interpreted to indicate that both ferrocene groups on the BFDMA molecule are oxidized at similar potentials. In addition, we note that we previously characterized a surfactant similar to BFDMA, $Fc(CH_2)_8N^+(CH_3)_2(CH_2)_3{-}(CH_3)_2N^+(CH_2)_8Fc\ 2Br^-$ at a gold electrode by CV.[51] Similar to the results reported in this article with BFDMA, we observed this surfactant to exhibit a single peak (in CVs), with a magnitude that varied with scan rate with an exponent between 0.55 and 0.78 (dependent on concentration: 0.01–1 mM).

The second observation arising from Figure 3 is that an estimate for the formal potential, E^o, for FTMA (0.140 ± 0.010 V, (vs. Ag|AgCl) calculated as the average of the anodic and cathodic peak potentials for diffusing species, i.e., $E^o = (E_{peak,a} + E_{peak,c})/2$) is lower than that of BFDMA [0.305 ± 0.004 V, (vs. Ag|AgCl)], indicating that the free energy required to change the oxidation state of FTMA is less than BFDMA by 18.3 ± 0.7 kT. We note that this difference in free energy is roughly twice that of the difference in free energy of aggregation of FTMA and BFDMA in bulk solution (~7 kT based on a CMC for FTMA of 0.1 mM[52] and a CMC for BFDMA of 1×10^{-7} M[31]). In addition, for BFDMA, we note the separation of the peak potentials, $E_{peak,a}$ and $E_{peak,c}$ to be 0.043 V at a scan rate of 10 mV/s. Because the peak separation for a reversible electrode process should be 0.059 V/n, where n is the number of electrons transferred,[53] this result provides further evidence that both ferrocene groups on each molecule of BFDMA are being oxidized during the anodic scan (see Supporting Information for a full discussion). We also note that the values of E^o described above for FTMA and BFDMA are generally consistent with those reported previously for these ferrocenyl surfactants (under conditions that differed from those reported in this article). For example, for FTMA, Liu et al.[54]

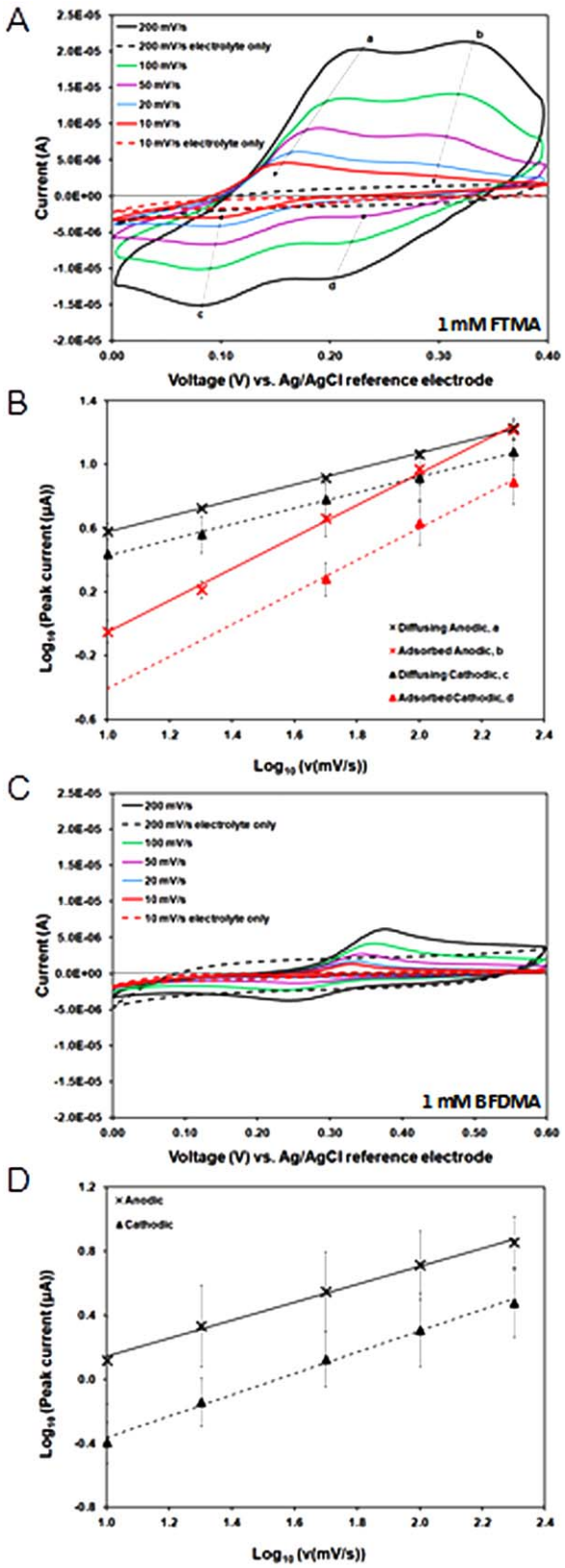

Figure 3.

Figure 3. Cyclic voltammograms of aqueous solutions of (A) 1 mM reduced FTMA and (C) 1 mM reduced BFDMA, in 1 mM Li_2SO_4 pH 5.

"Electrolyte only" refers to control experiments using 1 mM Li_2SO_4 free of amphiphile. A platinum disk working electrode (diameter of 5 mm), platinum mesh counter electrode, and a Ag|AgCl reference electrode were used. (B and D) Log–log plots of anodic or cathodic Faradaic peak currents vs. υ (correlation coefficient, $r^2 > 0.99$ for all fits). The dependence of the magnitude of the peak current on scan rate was characterized by an exponent of 0.50 ± 0.01 for each first (lines a and c) and 1.00 ± 0.01 for each second (lines b and d) anodic and cathodic peaks for FTMA ($n = 2$), and 0.57 ± 0.12 for the anodic peaks, and 0.67 ± 0.10 for the cathodic peaks of BFDMA ($n = 3$). [Color figure can be viewed in the online issue, which is available at wileyonlinelibrary.com.]

Table 1. DLS Analysis of Hydrodynamic Sizes of Aggregates Formed in Aqueous Solutions of 1 mM FTMA or 1 mM BFDMA in 1 mM Li_2SO_4

	Hydrodynamic Diameter, d_H (nm)		
Amphiphile	DLS	CV* via $i_{peak,a}$	RDE CV† via $i_{l,c}$
FTMA	10 ± 4	10	4
BFDMA	795 ± 250	700	n/a

Calculation of hydrodynamic sizes of aggregates using peak currents measured at stationary electrodes (Figure 3) using the Randles–Sevcik equation (Eq. 1)* or at rotating electrodes (Figure 5) using the Levich equation (Eq. 3),† followed by the use of Stokes–Einstein equation (Eq. 4) to calculate the hydrodynamic diameter.

reported CV data with an E^o value of 0.13–0.14 V (vs. Ag|AgCl) for FTMA (using a gold electrode and an electrolyte concentration of 0.1 M Li_2SO_4). For BFDMA, Kakizawa et al.[32] reported CV data with an E^o value of approximately 0.31 V (vs. Ag|AgCl, using platinum wire electrodes).

The third key observation that we make regarding the CVs of FTMA and BFDMA is that the magnitudes of the anodic and cathodic peak currents obtained using BFDMA are smaller than those of FTMA (e.g., at 200 mV/s, $i_{peak,a}$ is 6 μA for diffusing and adsorbed species of BFDMA but 19 μA for diffusing species of FTMA alone, see Figures 3A, C, solid black lines). If the currents were due solely to species diffusing from solution to the electrode, according to Eq. 1 this difference in current could be attributed to differences in the effective diffusion coefficients (D_o) (note that n is 1 for FTMA and 2 for BFDMA, Figure 1). By using the peak currents measured at 100 mV/s for both BFDMA and FTMA, we estimated the apparent diffusion coefficient, and thus the apparent hydrodynamic diameter (d_H, Table 1) of the assemblies diffusing to the electrodes. We note that, while we analyzed the peak corresponding to diffusing species for FTMA, the peak analyzed for BFDMA necessarily included current arising from both diffusing and adsorbed species (see above). We emphasize, therefore, that the apparent size of the aggregates of BFDMA is a lower bound to the actual size of the aggregates in solution. We note also that Eqs. 1–3 neglect the effects of local electric fields and transport of charge compensating ions, which can alter estimates of diffusion coefficients obtained from these equations particularly in the limit of low concentrations of electrolytes.[54] Efforts to perform experiments with BFDMA with concentrations of electrolytes greater than 1 mM Li_2SO_4 were prevented by insolubility of the BFDMA. For comparison, we also measured the hydrodynamic sizes of the aggregates using DLS (Table 1). Inspection of Table 1 reveals that values of d_H calculated from the peak anodic currents are in general agreement with the DLS data for each amphiphile (i.e., 10 ± 4 nm from DLS compared to 10 nm from $i_{peak,a}$ for FTMA, and 795 ± 250 nm from DLS compared to 700 nm from $i_{peak,a}$ for BFDMA).

Overall, the CVs shown in Figure 3 clearly establish that, for both FTMA and BFDMA, a population of each amphiphile is adsorbed to the electrodes and undergoes oxidation/reduction during the cycling of the electrode potential, with adsorbed and diffusing species separated during the voltage scan for FTMA but not for BFDMA. To provide information regarding the relative stability of the assemblies of adsorbed amphiphiles (FTMA or BFDMA) formed on the Pt electrode,

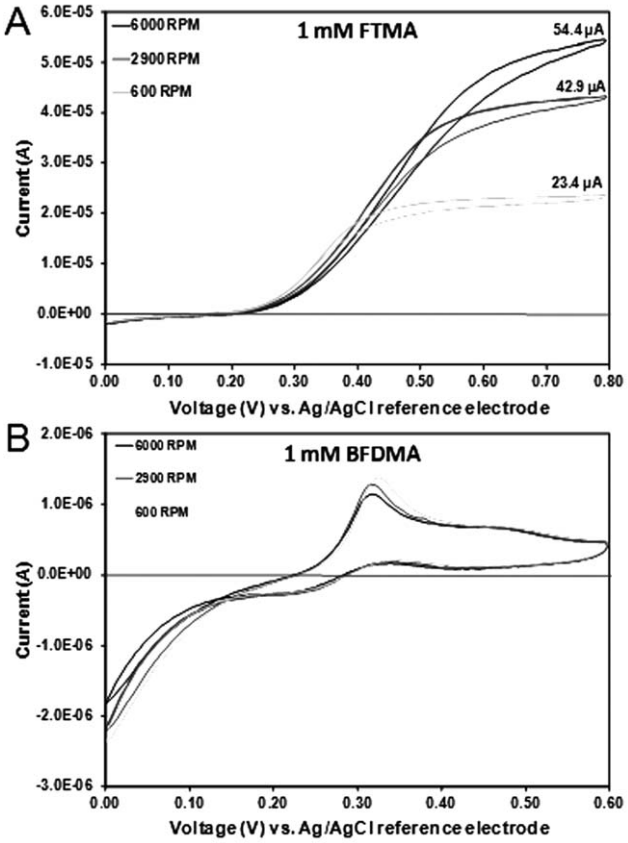

Figure 5. Linear sweep measurements obtained at a RDE for (A) 1 mM $FTMA_{RED}$ and (B) 1 mM $BFDMA_{RED}$, in 1 mM Li_2SO_4 pH 5.

The scan rate was 10 mV/s. A platinum disk working electrode (diameter of 5 mm), platinum mesh counter electrode, and a Ag|AgCl reference electrode were used.

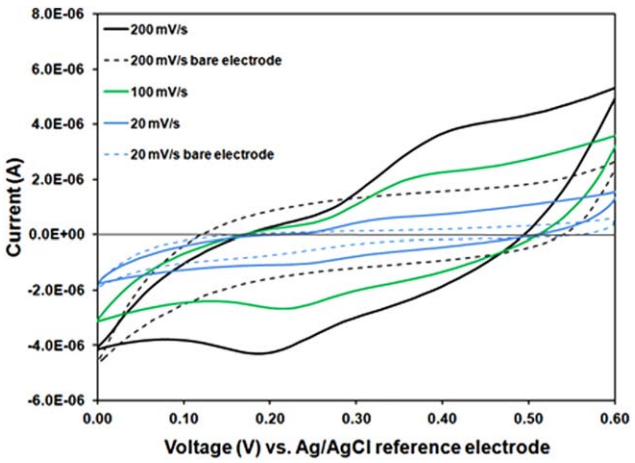

Figure 4. Cyclic voltammograms measured in aqueous 1 mM Li_2SO_4 after incubation of a Pt working electrode in a solution of 1 mM BFDMA in 1 mM Li_2SO_4.

Upon removal from the solution of BFDMA, the working electrode was gently rinsed with 1 mM Li_2SO_4 and immersed in the solution of 1 mM Li_2SO_4. A platinum disk working electrode (diameter of 5 mm), platinum mesh counter electrode, and a Ag|AgCl reference electrode were used. [Color figure can be viewed in the online issue, which is available at wileyonlinelibrary.com.]

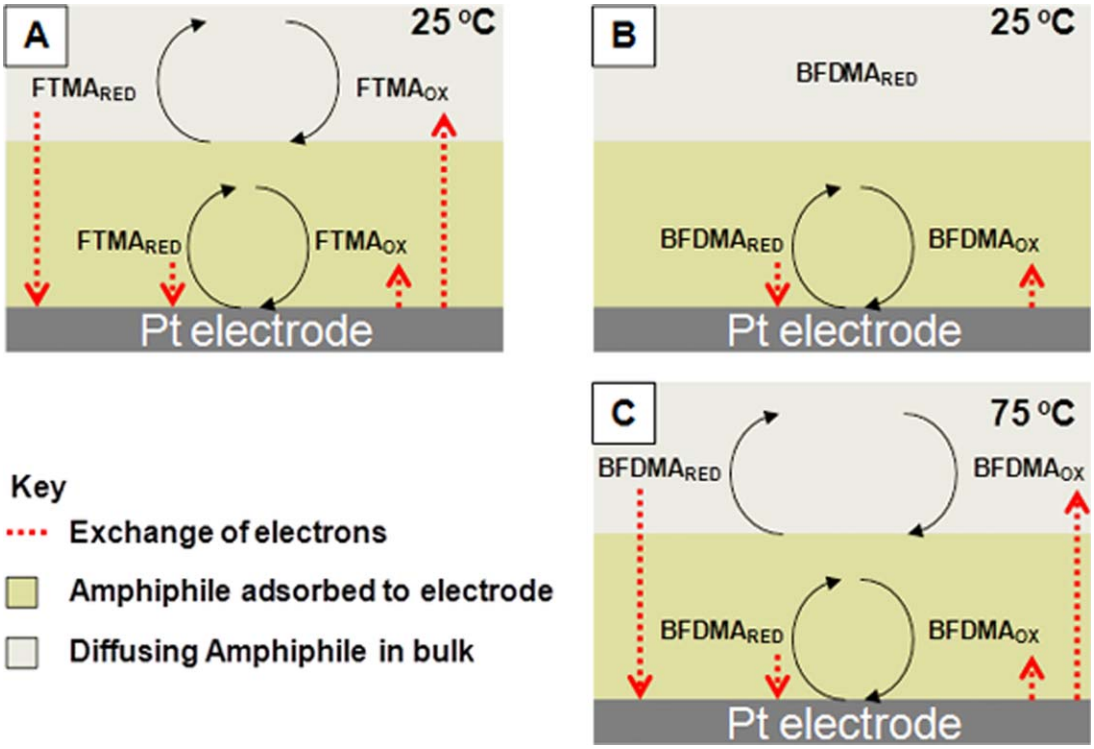

Scheme 1. Electrochemical activity during a complete CV scan for adsorbed and diffusing (A) FTMA at 25°C, (B) BFDMA at 25°C, and (C) BFDMA at 75°C.

[Color figure can be viewed in the online issue, which is available at wileyonlinelibrary.com.]

we measured CVs at Pt electrodes in solutions of either FTMA or BFDMA (as described earlier in the context of the electrode conditioning) and then transferred the electrodes to 1 mM Li_2SO_4 solutions that were free of dissolved amphiphiles. Figure 4 shows that, upon scanning of the potential of the pre-treated electrodes in the electrolyte solution free of amphiphile, Faradaic peaks were measured in both scan directions for BFDMA. In contrast, in a similar experiment performed with FTMA, no such current peaks were measurable (see Supporting Information Figure S3). We analyzed the magnitude of the anodic peaks for BFDMA in Figure 4. We then calculated the surface concentration of accessible BFDMA (Γ_o) to be between 4.9 and 12.2 nm^2/molecule using Eq. 2. The magnitudes of the anodic and cathodic Faradaic peaks associated with the adsorbed BFDMA (Figure 4) were approximately 33–40% of those measured when the CVs were recorded in the bulk solutions of BFDMA (equivalent scan rate data, Figure 3C). This result is consistent with our conclusion, based on the scan rate dependence of the peak current shown in Figure 3C, that the peak current measured in the bulk solution of BFDMA contained contributions from both adsorbed and diffusing species.

A surprising result, however, was obtained when the scan rate of the potential was varied in the experiment in Figure 4. We measured the magnitude of the peak current to change with scan rate with an exponent of 0.59 for $i_{peak,a}$ and 0.57 for $i_{peak,c}$, consistent with the presence of both diffusing species and adsorbed species. Because the BFDMA in bulk solution was removed in this experiment, we hypothesized that the flux of BFDMA to the electrode was influenced by the diffusion of BFDMA within an adsorbed layer or film of BFDMA that persists at the electrode after rinsing and transfer to a solution of 1 mM Li_2SO_4. In contrast, there is no evidence of FTMA at the surface of the electrode following an equivalent rinse (Supporting Information Figure S3).

Linear sweep voltammetry at a RDE

As discussed above, we interpreted the CVs obtained at the stationary electrode to indicate that both BFDMA and FTMA adsorb onto the electrode. The adsorbed layer of BFDMA appears to attenuate the contribution of BFDMA in bulk solution to the CV, although the scan-rate-dependence of the CV also suggests that BFDMA is mobile (diffusing) within the adsorbed layer at the electrode (Figures 3 and 4). In contrast, FTMA adsorbed to the electrode, while evident in the CV as a distinct peak, does not appear to block substantially the flux of FTMA to the electrode from bulk solution (see Scheme 1A). To provide an additional test of the physical picture that emerges from CV at the stationary electrode, we performed linear sweep voltammetry at a RDE.

Figure 5 shows voltammograms of FTMA (Figure 5A) and BFDMA (Figure 5B) obtained at an electrode undergoing rotation at three different speeds (either 600, 2900, or 6000 rpm). An initial inspection of the CVs in Figure 5A suggests that solutions of FTMA (Figure 5A) follow a typical Levich-type current behavior (Eq. 3), that is, a mass transfer-limited rate of oxidation at the electrode. In brief, in this scenario, the fluid convection driven by the motion of the working electrode causes reactants of the half-cell reaction to be replenished at the surface of the electrode, thus avoiding any significant depletion of the concentration of redox species at the electrode (as occurs with a stationary electrode).[53] In addition, it is evident from Figure 5A that the magnitude of the peak current increased with rotational speed of the working electrode and that the difference

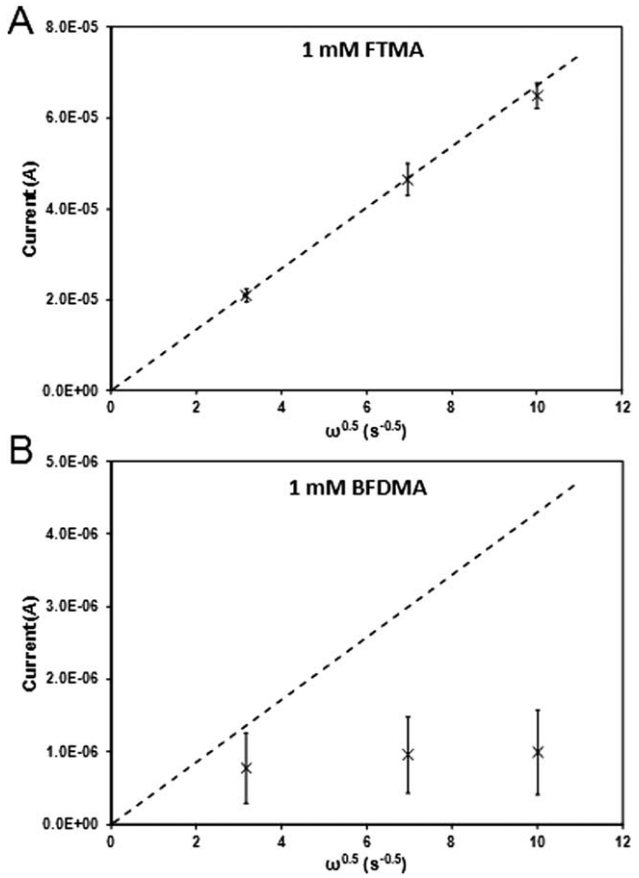

Figure 6. Peak anodic currents measured at RDEs using (A) 1 mM FTMA or (B) 1 mM BFDMA, in 1 mM Li_2SO_4 pH 5.

For each graph, (*x*) represents the experimental data and the dotted line is the Levich current. See text for a full description of parameters used to model each analyte. The scan rate was 10 mV/s. A platinum disk working electrode (diameter of 5 mm), platinum mesh counter electrode, and a Ag|AgCl reference electrode were used. Error bars represent one standard deviation ($n = 3$).

between current passed at the electrode during the anodic and cathodic sweeps (at 10 mV/s) is small.

In contrast to FTMA, solutions of BFDMA (Figure 5B) generated voltammograms at the RDE that possessed a Faradaic current peak during the anodic voltage scan. This peak was evident for all rotation speeds of the working electrode (i.e., from 600 to 6000 rpm). The presence of the peak indicates that the BFDMA that was oxidized at the electrode was not replenished during the anodic scan. This interpretation is consistent with the presence of an adsorbed layer of BFDMA that serves as a barrier to the convective transport of BFDMA from bulk solution to the electrode (see Scheme 1B). Also in contrast to FTMA, we note that the cathodic scans obtained with BFDMA differed substantially from the anodic scans. This result is also consistent with the presence of an adsorbed assembly of BFDMA that is oxidized during the anodic scan.

The magnitude of the Faradaic peak current measured during the anodic scan of BFDMA (Figure 5B) provides further insight to the influence of the adsorbed layer of BFMDA on processes occurring at the electrode. The peak current measured at the RDE was 1.0–1.3 μA, which is comparable to the peak current measured at the stationary electrode at the equivalent scan rate (1.0 μA for 10 mV/s; Figure 3C, red solid line). This observation again suggests that the Faradaic peak current is produced predominantly from electroactive species that are locally diffusing to and from the electrode within large aggregates of BFDMA (see Scheme 1B), as would be expected if the electrode were not rotating and forcing a constant supply of reactants to the surface of the electrode. In addition, we note that with increasing scan rate, the magnitude of the peak current in Figure 5B decreases. Although we do not yet fully understand the origins of this phenomenon, we hypothesize that large aggregates of BFDMA (795 ± 250 nm, Table 1) may be loosely bound to the electrode surface, adding to the localized population of slowly diffusing BFDMA molecules that contribute to the Faradaic current. As rotation speed increases, we speculate that the shear force imposed on these weakly adsorbed aggregates of BFDMA may increase, leading to their removal from the electrode and a lowering of the peak current.

Figure 6 shows the limiting anodic current passed at the RDE immersed into solutions of either FTMA or BFDMA plotted against $\omega^{1/2}$ (as per Eq. 3) to quantitatively compare each amphiphile to Levich-type behavior. For both amphiphiles, the calculated Levich current is shown as a dotted line. The Levich current in Figure 6A (for FTMA) was calculated using a hydrodynamic diameter of 4 nm (similar to DLS data of 10 ± 4 nm, see Table 1). The agreement between the model and the experimental data (crosses, Figure 6A) is good, thus confirming that the rate of oxidation of FTMA is mass transfer-limited. For BFDMA (Figure 6B), the Levich current calculated assuming a hydrodynamic diameter of 700 nm (obtained from the DLS data in Table 1) greatly exceeds the experimentally measured currents. This observation is consistent with our conclusion that the current passed at the electrode immersed into the BFDMA solution is not limited by mass transfer from the bulk solution.

In summary, our analyses of the linear sweep voltammograms measured at the RDE lead to a physical picture that is consistent with that suggested by our CV measurements at the stationary electrode. Specifically, both sets of experiments support the proposition that the current passed at the electrode in the presence of BFDMA is dominated by BFDMA that is within an adsorbed assembly at the surface of the electrode. Also, the RDE experiments suggest that diffusion of BFDMA from aggregates outside of the adsorbed layer plays little role in determining the current passed at the electrode (Scheme 1B). There does, however, appear to be a population of BFDMA aggregates that are weakly bound to the electrode and can be removed by shear. In contrast, RDE experiments with FTMA show typical mass transfer-limited Levich-type behavior (Scheme 1A).

Investigation of the effects of heating BFDMA

To investigate further the physical state of the adsorbed layer of BFDMA that appears to regulate the rate of oxidation of BFDMA (see above), we explored the effects of heating solutions of BFDMA. First, we performed measurements using DSC to determine if BFDMA exhibits evidence of a melting transition. Figure 7 shows the heat flow during a 1°C/min ramp of solutions of either 1 mM FTMA or 1 mM BFDMA (between 25 and 85°C or 80°C, respectively). Although the scans obtained using FTMA were featureless

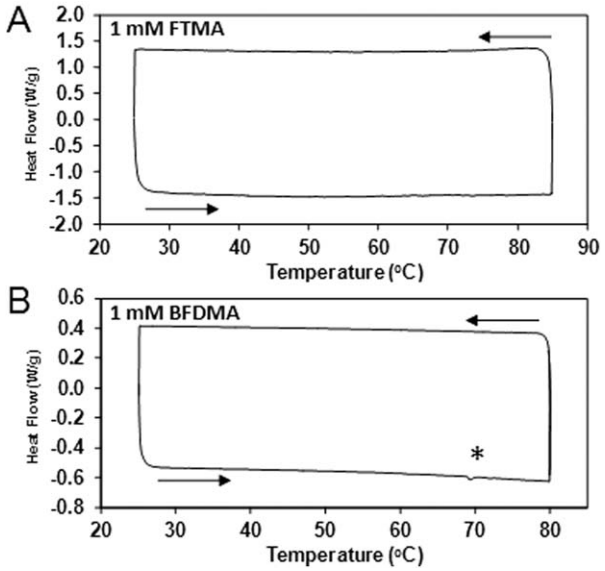

Figure 7. Thermograms obtained by DSC of aqueous solutions of (A) 1 mM FTMA or (B) 1 mM BFDMA, in 1 mM Li_2SO_4.

The temperature was changed at a rate of 1°C/min in both scan directions. An asterisk, * shows a small endothermic peak upon heating of 1 mM BFDMA with an onset at 68.95°C and a maximum at 69.33°C.

(Figure 7A), an endothermic event was recorded for BFDMA (asterisk, Figure 7B) during the increase in temperature. The endothermic event started at a temperature of 68.95°C, peaked at 69.33°C, and corresponded to an overall molar enthalpy of 96.7 kJ/mol of BFDMA. Here, we note that the magnitude of the molar enthalpy measured for BFDMA is comparable to that measured previously for the gel-to-liquid transition (45.9 kJ/mol at 44°C) of dioctadecyldimethylammonium bromide (DODAB),[55] an amphiphile with a structure that is similar to BFDMA but without the terminal ferrocene groups. We also measured the hydrodynamic size of BFDMA as a function of temperature using DLS. The average hydrodynamic diameter of BFDMA at 75°C was measured to be 565 ± 40 nm, a drop in size of 230 nm from that measured at 25°C. These observations, when combined, suggest that the melting of the BFDMA aggregates is accompanied by redistribution of the BFDMA among the aggregates in solution. We also note that we did not detect an exothermic process (i.e., freezing) when a solution of BFDMA was cooled from 75 to 25°C (Figure 7B). We interpret this result to indicate that either the melting transition was not reversible on the time-scale of our experiments, or that a process of freezing does occur but that it occurs over a broad temperature range that makes it difficult to detect.

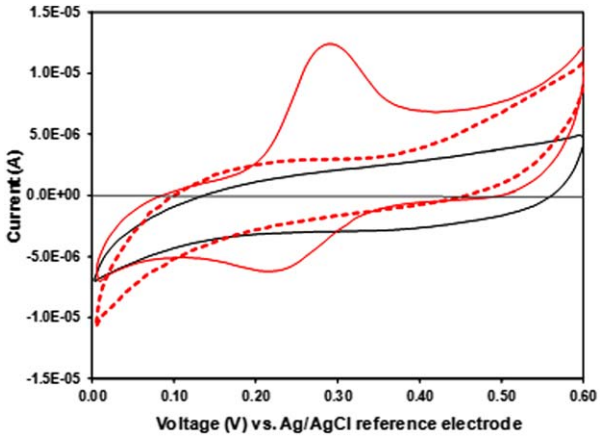

Figure 8. Cyclic voltammograms measured at a stationary electrode immersed into 1 mM Li_2SO_4 (dashed red line), then 1 mM reduced BFDMA in 1 mM Li_2SO_4 at 75°C (red line), and then 1 mM Li_2SO_4 at 25°C (black line), at a scan rate of 100 mV/s.

[Color figure can be viewed in the online issue, which is available at wileyonlinelibrary.com.]

The latter interpretation is supported by DLS analysis of a solution of 1 mM BFDMA, preheated to 75°C for 2 h and then allowed to cool to room temperature. An analysis of the size distribution reveals an average mean diameter of 706 ± 20 nm, that is, similar to a solution of 1 mM BFDMA that has not been preheated (795 ± 250 nm, Table 1), suggesting that the self-assembly processes occurring in solution upon heating are reversible.

To determine whether the above-described change in phase state of BFDMA had a measurable impact on the electrochemical activity of adsorbed and/or diffusing species of BFDMA, we performed electrochemical measurements at stationary and RDEs as a function of temperature. The CVs at stationary electrodes were measured at 60 and 75°C, above or below the endothermic event observed in Figure 7B, in an experiment otherwise identical to that reported in Figure 3C. Table 2 shows the results of these experiments (see Supporting Information Figure S4, for the CVs). Similar to the CVs reported at ambient temperature, at both elevated temperatures one Faradaic peak was observed in each scan direction. In addition, the peak currents changed with scan rate with an exponent between 0.5 and 1.0 (see Table 2 for calculated values), thus confirming the presence of adsorbed and diffusing electroactive species. However, increasing the temperature from 25 to 60°C or 75°C also led to several differences in the CV relative to what was observed at ambient temperatures. First, the Faradaic peak currents measured in

Table 2. Peak potentials and Currents Obtained from CVs of Either 1 mM FTMA (Lowest Potential Peaks in Each Scan Direction Only, Figure 3A) or 1 mM BFDMA (Figure 3C and Supporting Information Figure S4) in 1 mM Li_2SO_4 at a Scan Rate of 100 mV/s

Amphiphile	Temperature (°C)	$E_{peak,a}$(V)	$E_{peak,c}$ (V)	E^o (V)	$i_{peak,a}$ (μA)	$i_{peak,c}$ (μA)	a_a	a_c
FTMA	25	0.21	0.08	0.15	12.0	−10.3	0.50	0.50
BFDMA	25	0.36	0.26	0.31	3.3	−1.1	0.57	0.67
	60	0.28	0.24	0.26	3.6	−2.0	0.55	0.78
	75	0.28	0.22	0.25	9.2	−5.0	0.59	0.85
	25 (preheated to 75°C)	0.39	0.25	0.32	4.0	−2.7	0.51	0.58

Values of a_a and a_c were calculated from a range of scan rates between 10 and 200 mV/s. R^2 of a_a and a_c values are >0.99.

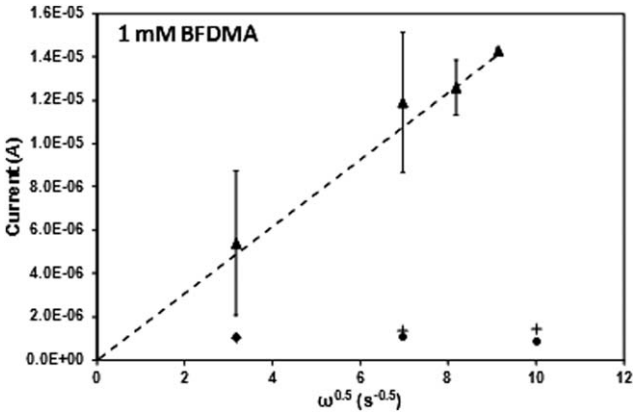

Figure 9. Peak anodic currents measured at a RDE immersed in aqueous 1 mM BFDMA containing 1 mM Li_2SO_4 pH 5 upon heating to 60°C (+) or 75°C (▲) and upon preheating to 75°C (•) (2 h incubation) then cooling to 25°C, respectively.

The dotted line corresponds to a Levich current (see text for details). The scan rate was 10 mV/s. A platinum disk working electrode (diameter of 5 mm), platinum mesh counter electrode, and a Ag|AgCl reference electrode were used. Error bars represent one standard deviation ($n = 3$).

both scan directions increased significantly at 75°C but not at 60°C. For example, at 75°C and at 100 mV/s, $i_{peak,a}$ increased from 3.3 to 9.2 μA, and $i_{peak,c}$ increased in magnitude from −1.1 to −5.0 μA when compared to CV measurements at 25°C. In contrast, at 60°C, the magnitude of the current peaks remained low, with an $i_{peak,a}$ of 3.6 μA and $i_{peak,c}$ of −2.0 μA. This result indicates that the rate of oxidation of BFDMA is higher at 75°C than at ambient temperature or 60°C, consistent with the melting of BFDMA aggregates at 69°C. Second, we measured E^o to decrease from 0.31 V (vs. Ag|AgCl) at 25°C to 0.26 V (vs. Ag|AgCl) at 60°C and to 0.25 V (vs. Ag|AgCl) at 75°C, that is, the change in free energy required to change the oxidation state of BFDMA was measured to decrease at these higher temperatures. The change in E^o with temperature, however, does not appear to be due to the difference in the phase state of the adsorbed BFDMA at the surface of the electrode. Third, we also performed CVs in 1 mM Li_2SO_4 solutions following pretreatment of the electrode in 1 mM BFDMA at 75°C to determine whether adsorbed BFDMA persists at the electrode at this temperature. The CV measured in the 1 mM Li_2SO_4 solution showed no evidence of a Faradaic peak in either scan direction (Figure 8), in contrast to the result in Figure 4 where an otherwise identical experiment was performed at 25°C. This result is consistent with removal of the adsorbed layer of BFDMA upon transfer into the 1 mM Li_2SO_4 solution at this higher temperature (similar to FTMA at ambient temperatures).

Next, we performed measurements at a RDE at 60 and 75°C (Figure 9 and Supporting Information Figure S5). At 75°C, the peak currents measured with BFDMA followed a Levich current behavior with a corresponding hydrodynamic diameter of 80 nm (using Eq. 3). This diameter is significantly lower than the hydrodynamic diameter of 705 ± 250 nm measured using DLS (see above). We note, however, that the BFDMA aggregates are polydisperse, and it is also possible that shear within the boundary layer of the RDE may break up loose aggregates of the BFDMA. In contrast, at 60°C, the qualitative behavior of the peak currents was similar to that observed at 25°C (Figure 6B). That is, the magnitudes of the anodic currents were not strongly dependent on rotational speed, and a peak in the current was seen during the anodic scan. These results support the conclusion emerging from the DSC that BFDMA undergoes a melting transition between 60 and 75°C, and that the CVs of BFDMA measured at 25°C are dominated by aggregates of BFDMA that adsorb to the surface of the electrode.

Finally, we performed bulk electrolysis of a solution of BFDMA at 75°C at an oxidizing potential of 0.6 V (vs. Ag|AgCl) in an otherwise identical electrochemical experiment to that reported in Figure 2. We measured a charge of 0.868 C (i.e., 100% conversion to oxidized BFDMA) to be passed at the electrode after 2.7 h. This result, when compared to the data in Figure 2, reveals the rate of oxidation of BFDMA at 75°C to be approximately 13 times faster than at 25°C (and only 1.5 times slower than FTMA at 25°C). This result supports our conclusion that at 75°C, while BFDMA is still adsorbed to the surface of the working electrode, the adsorbed assembly does not block access of BFDMA in bulk solution to the electrode (see Scheme 1C). In contrast, at 60°C, the adsorbed BFDMA influences electrode processes in a manner similar to that measured at 25°C. The data collected at elevated temperatures on either side of the endothermic event identified via DSC (Figure 7B) show the pronounced effect of the phase state of the BFDMA assemblies on the electrochemical characteristics of redox-active amphiphiles.

The results described above suggest that solution conditions (or, e.g., the addition of cosurfactants, salts, or acids) that change the phase state of the amphiphiles will substantially impact electrode processes involving BFDMA, leading to facile oxidation and reduction via electrochemical methods. More broadly, the results presented in this article, which identify the phase state of redox-active amphiphiles at interfaces as playing a central role in electron transfer processes involving those amphiphiles, provide guidance for the design of self-assembling redox mediators that offer the potential for broad control of interfacial charge separation processes. The results also enable electrochemical approaches for control of surfactant-based phenomena using ferrocenyl amphiphiles, including control of the formation of complexes between BFDMA and DNA in the context of development of methods that permit spatial and temporal control over the delivery of genes to cells.[26–30]

Conclusions

In conclusion, this study provides insights into the influence of the dynamics of self-assembled redox-active amphiphiles on their electrochemical activities. Specifically, we focused on comparing two ferrocene-containing amphiphiles that we reveal to exhibit strikingly different electrochemical signatures via CV at stationary and rotating electrodes. Although both amphiphiles form interfacial assemblies on Pt electrodes at ambient conditions, the dynamics of the adsorbed FTMA are fast, and the interfacial assembly of the surfactant has little impact on the access of FTMA in bulk solution to the electrode. The rate limiting process for this amphiphile at the RDE is mass transport from the bulk solution. In contrast, the behavior of BFDMA is more complex.

Specifically, at ambient temperatures, there exists a bound layer of BFDMA that is not displaced from the surface by gentle rinsing. Measurements performed at the RDE indicate that the bound layer of BFDMA largely blocks the contributions of BFDMA in bulk solution to the current passed at the electrodes. However, CV performed at a stationary electrode as a function of scan rate reveals that BFDMA is diffusing within the adsorbed layer. Finally, DSC measurements indicated that BFDMA undergoes a melting transition of some type at 69°C, and subsequent investigation revealed that the electrochemical traits of BFDMA above the melting transition were similar to that of FTMA (see Scheme 1). Overall, these results indicate that the dynamic properties of assemblies formed by ferrocenyl amphiphiles play a dominant role in determining their electrochemical activity.

Acknowledgments

Financial support was provided by National Science Foundation (CBET-1263970), the National Institutes of Health (AI092004, EB006168), and the ARO (W911NF-11-1-0251). Use of the shared experimental facilities of the MRSEC (DMR-1121288) is gratefully acknowledged.

Literature Cited

1. Fedurco M. Redox reactions of heme-containing metalloproteins: dynamic effects of self-assembled monolayers on thermodynamics and kinetics of cytochrome c electron-transfer reactions. *Coord Chem Rev*. 2000;209:263–331.
2. Nassar AEF, Rusling JF, Nakashima N. Electron transfer between electrodes and heme proteins in protein-DNA films. *J Am Chem Soc*. 1996;118(12):3043–3044.
3. Mitschke U, Bauerle P. The electroluminescence of organic materials. *J Mater Chem*. 2000;10(7):1471–1507.
4. Peumans P, Yakimov A, Forrest SR. Small molecular weight organic thin-film photodetectors and solar cells. *J Appl Phys*. 2003;93(7):3693–3723.
5. Friend RH, Gymer RW, Holmes AB, Burroughes JH, Marks RN, Taliani C, Bradley DDC, Santos DAD, Bredas JL, Logdlund M, Salaneck WR. Electroluminescence in conjugated polymers. *Nature*. 1999;397(6715):121–128.
6. Chen J, Reed MA, Rawlett AM, Tour JM. Large on-off ratios and negative differential resistance in a molecular electronic device. *Science*. 1999;286(5444):1550–1552.
7. Malka A, Peskin U. Langevin-Schroedinger formulation of electronic tunneling through a molecular bridge with a dissipative acceptor. *Isr J Chem*. 2005;45(1–2):217–225.
8. Morad MS, Sarhan AAO. Application of some ferrocene derivatives in the field of corrosion inhibition. *Corros Sci*. 2008;50(3):744–753.
9. Ma HY, Chen SH, Yin BS, Zhao SY, Liu XQ. Impedance spectroscopic study of corrosion inhibition of copper by surfactants in the acidic solutions. *Corros Sci*. 2003;45(5):867–882.
10. Wang X, Hsing IM. Surfactant stabilized Pt and Pt alloy electrocatalyst for polymer electrolyte fuel cells. *Electrochim Acta*. 2002;47(18):2981–2987.
11. Franklin TC, Ohta M. Voltammetric studies using a hyamine-2389 polystyrene-filmed electrode. *Surf Technol*. 1983;18(1):63–76.
12. Chidsey CED. Free-energy and temperature-dependence of electron-transfer at the metal-electrolyte interface. *Science*. 1991;251(4996):919–922.
13. Sikes HD, Smalley JF, Dudek SP, Cook AR, Newton MD, Chidsey CED, Feldberg SW. Rapid electron tunneling through oligophenylenevinylene bridges. *Science*. 2001;291(5508):1519–1523.
14. Slowinski K, Fong HKY, Majda M. Mercury-mercury tunneling junctions. 1. Electron tunneling across symmetric and asymmetric alkanethiolate bilayers. *J Am Chem Soc*. 1999;121(31):7257–7261.
15. Slowinski K, Slowinska KU, Majda M. Electron tunnelling across hexadecanethiolate monolayers on mercury electrodes: reorganization energy, structure, and permeability of the alkane/water interface. *J Phys Chem B*. 1999;103(40):8544–8551.
16. Charych DH, Landau EM, Majda M. Electrochemistry at the air-water interface—lateral diffusion of an octadecylferrocene amphiphile in langmuir monolayers. *J Am Chem Soc*. 1991;113(9):3340–3346.
17. Miller JR, Beitz JV. Long-range transfer of positive charge between dopant molecules in a rigid glassy matrix. *J Chem Phys*. 1981;74(12):6746–6756.
18. Sachs SB, Dudek SP, Hsung RP, Sita LR, Smalley JF, Newton MD, Feldberg SW, Chidsey CED. Rates of interfacial electron transfer through pi-conjugated spacers. *J Am Chem Soc*. 1997;119(43):10563–10564.
19. Newton MD. Quantum chemical probes of electron transfer kinetics—nature of the donor-acceptor interactions *Chem Rev*. 1991;91(5):767–792.
20. Abbott AP, Gounili G, Bobbitt JM, Rusling JF, Kumosinski TF. Electron-transfer between amphiphilic ferrocenes and electrodes in cationic micellar solution. *J Phys Chem*. 1992;96(26):11091–11095.
21. Liu XY, Abbott NL. Spatial and temporal control of surfactant systems. *J Colloid Interface Sci*. 2009;339(1):1–18.
22. Gallardo BS, Gupta VK, Eagerton FD, Jong LI, Craig VS, Shah RR, Abbott NL. Electrochemical principles for active control of liquids on submillimeter scales. *Science*. 1999;283(5398):57–60.
23. Gallardo BS, Hwa MJ, Abbott NL. In-situ and reversible control of the surface-activity of ferrocenyl surfactants in aqueous solutions. *Langmuir*. 1995;11(11):4209–4212.
24. Aydogan N, Abbott NL. Comparison of the surface activity and bulk aggregation of ferrocenyl surfactants with cationic and anionic headgroups. *Langmuir*. 2001;17(19):5703–5706.
25. Hays ME, Abbott NL. Electrochemical control of the interactions of polymers and redox-active surfactants. *Langmuir*. 2005;21(25):12007–12015.
26. Aytar BS, Muller JPE, Golan S, Hata S, Takahashi H, Kondo Y, Talmon Y, Abbott NL, Lynn DM. Addition of ascorbic acid to the extracellular environment activates lipoplexes of a ferrocenyl lipid and promotes cell transfection. *J Control Release*. 2012;157(2):249–259.
27. Abbott NL, Jewell CM, Hays ME, Kondo Y, Lynn DM. Ferrocene-containing cationic lipids: influence of redox state on cell transfection. *J Am Chem Soc*. 2005;127(33):11576–11577.
28. Jewell CM, Hays ME, Kondo Y, Abbott NL, Lynn DM. Ferrocene-containing cationic lipids for the delivery of DNA: oxidation state determines transfection activity. *J Control Release*. 2006;112(1):129–138.
29. Jewell CM, Hays ME, Kondo Y, Abbott NL, Lynn DM. Chemical activation of lipoplexes formed from DNA and a redox-active, ferrocene-containing cationic lipid. *Bioconjug Chem*. 2008;19(11):2120–2128.
30. Pizzey CL, Jewell CM, Hays ME, Lynn DM, Abbott NL, Kondo Y, Golan S, Talmon Y. Characterization of the nanostructure of complexes formed by a redox-active cationic lipid and DNA. *J Phys Chem B*. 2008;112(18):5849–5857.
31. Yoshino N, Shoji H, Kondo Y, Kakizawa Y, Sakai H, Abe M. Syntheses of cationic surfactants having two ferrocenylalkyl chains. *J Jpn Oil Chem Soc*. 1996;45:769–775.
32. Kakizawa Y, Sakai H, Yamaguchi A, Kondo Y, Yoshino N, Abe M. Electrochemical control of vesicle formation with a double-tailed cationic surfactant bearing ferrocenyl moieties. *Langmuir*. 2001;17(26):8044–8048.
33. Muller JPE, Aytar BS, Kondo Y, Lynn DM, Abbott NL. Incorporation of DOPE into lipoplexes formed from a ferrocenyl lipid leads to inverse hexagonal nanostructures that allow redox-based control of transfection in high serum. *Soft Matter*. 2012;8(24):2608–2619.
34. Bennett DE, Gallardo BS, Abbott NL. Dispensing surfactants from electrodes: marangoni phenomenon at the surface of aqueous solutions of (11-ferrocenylundecyl)trimethylammonium bromide. *J Am Chem Soc*. 1996;118(27):6499–6505.
35. Rosslee CA, Abbott NL. Principles for microscale separations based on redox-active surfactants and electrochemical methods. *Anal Chem*. 2001;73(20):4808–4814.
36. Liu XY, Abbott NL. Electrochemical generation of gradients in surfactant concentration across microfluidic channels. *Anal Chem*. 2009;81(2):772–781.
37. Liu XY, Abbott NL. Lateral transport of solutes in microfluidic channels using electrochemically generated gradients in redox-active surfactants. *Anal Chem*. 2011;83(8):3033–3041.
38. Aytar BS, Muller JPE, Golan S, Hata S, Takahashi H, Kondo Y, Talmon Y, Abbott NL, Lynn DM. Addition of ascorbic acid to the extracellular environment activates lipoplexes of a ferrocenyl lipid and promotes cell transfection. *J Control Release*. 2012;157:249–259.

39. Aytar BS, Muller JPE, Golan S, Kondo Y, Talmon Y, Abbott NL, Lynn DM. Chemical oxidation of a redox-active, ferrocene-containing cationic lipid: influence on interactions with DNA and characterization in the context of cell transfection. *J Colloid Interface Sci*. 2012;387(1):56–64.
40. Hays ME, Jewell CM, Kondo Y, Lynn DM, Abbott NL. Lipoplexes formed by DNA and ferrocenyl lipids: effect of lipid oxidation state on size, internal dynamics, and zeta-potential. *Biophys J*. 2007; 93(12):4414–4424.
41. Szanto DA, Cleghorn S, Ponce-De-Len C, Walsh FC. The limiting current for reduction of ferricyanide ion at nickel: the importance of experimental conditions. *AIChE J*. 2008;54(3):802–810.
42. Takei T, Sakai H, Kondo Y, Yoshino N, Abe M. Electrochemical control of solubilization using a ferrocene-modified nonionic surfactant. *Colloid Surf A Physicochem Eng Asp*. 2001;183:757–765.
43. Faulkner B. *Electrochemical Methods; Fundamentals and Applications*, 1st ed. New York: Wiley, 1980:231.
44. Faulkner B. *Electrochemical Methods; Fundamentals and Applications*, 1st ed. New York: Wiley, 1980:591.
45. Cochran WG. The flow due to a rotating disc. *Math Proc Cambridge Philos Soc*. 1934;30(3):365–375.
46. Levich VG. Physicochemical Hydrodynamics. Englewood Cliffs, NJ: Prentice-Hall, 1962.
47. Provencher SW. A constrained regularization method for inverting data represented by linear algebraic or integral equations *Comput Phys Commun*. 1982;27(3):213–227.
48. Provencher SW. CONTIN. *Comput Phys Commun*. 1982;27(3):229–242.
49. Faulkner B. *Electrochemical Methods; Fundamentals and Applications*, 1st ed. New York: Wiley, 1980:596.
50. Faulkner B. *Electrochemical Methods; Fundamentals and Applications*, 1st ed. New York: Wiley, 1980:36.
51. Gallardo BS, Abbott NL. Active control of interfacial properties: a comparison of dimeric and monomeric ferrocenyl surfactants at the surface of aqueous solutions. *Langmuir*. 1997;13(2):203–208.
52. Gallardo BS, Metcalfe KL, Abbott NL. Ferrocenyl surfactants at the surface of water: principles for active control of interfacial properties. *Langmuir*. 1996;12(17):4116–4124.
53. Faulkner B. *Electrochemical Methods; Fundamentals and Applications*, 1st ed. New York: Wiley, 1980.
54. Liu XY, Graham MD, Abbott NL. Methods for generation of spatial gradients in concentration of monomeric surfactants and micelles in microfluidic systems. *Langmuir*. 2007;23(19):9578–9585.
55. Cocquyt J, Olsson U, Ofsson G, Van der Meeren P. Thermal transitions of DODAB vesicular dispersions. *Colloid Polym Sci*. 2005; 283(12):1376–1381.

Manuscript received Oct. 16, 2013, and revision received Jan. 28, 2014.